Results in Engineering 22 (2024) 102237

Contents lists available at ScienceDirect

Results in Engineering

journal homepage: www.sciencedirect.com/journal/results-in-engineering

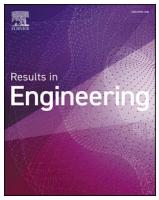

Electrical conductivity enhancement of rGO-MoS_2 composite electrode for inverted PSC by parameter optimization

Nur Ezyanie Safie [a,b], Mohd Asyadi Azam [b,c,*], Faiz Arith [d], T. Joseph Sahaya Anand [b], Najmiah Radiah Mohamad [d], Akito Takasaki [e]

[a] Fakulti Teknologi Dan Kejuruteraan Elektrik, Universiti Teknikal Malaysia Melaka, Hang Tuah Jaya, 76100, Durian Tunggal, Melaka, Malaysia
[b] Fakulti Teknologi Dan Kejuruteraan Industri Dan Pembuatan, Universiti Teknikal Malaysia Melaka, Hang Tuah Jaya, 76100, Durian Tunggal, Melaka, Malaysia
[c] Center for Promotion of Educational Innovation, Shibaura Institute of Technology, 3-7-5 Toyosu, Koto-ku, Tokyo, 135-8548, Japan
[d] Fakulti Teknologi Dan Kejuruteraan Elektronik Komputer, Universiti Teknikal Malaysia Melaka, Hang Tuah Jaya, 76100, Durian Tunggal, Melaka, Malaysia
[e] Department of Engineering Science and Mechanics, Shibaura Institute of Technology, 3-7-5 Toyosu, Koto-ku, Tokyo, 135-8548, Japan

ARTICLE INFO

Keywords:
Electrode fabrication
Parameter optimization
Electrical conductivity
Taguchi method
rGO-MoS_2 composite
Electrode material

ABSTRACT

Carbon-based electrodes are widely used in photovoltaic, metal-ion batteries, supercapacitors, and sensors due to their low ohmic resistance and ability to integrate modifiers. Reduced graphene oxide (rGO) represents a promising alternative to graphite in carbon-based electrodes because of its high electrical conductivity, large surface area, and robust mechanical properties. This study aimed to optimize the fabrication parameters of rGO-MoS_2 composite electrodes prepared via a one-pot hydrothermal method, focusing on maximizing their electrical conductivity for potential electronic applications. Taguchi analysis was employed to evaluate the impact of three key factors: rGO-MoS_2 mixing ratio, annealing temperature, and annealing time. The novelty of this work lies in the systematic optimization approach using the Taguchi method, which allowed for the identification of the most significant factors and their optimal levels. The optimal combination was found to be a 1:1 ratio, 75 °C annealing temperature, and 15-min annealing time, resulting in an impressive electrical conductivity of 11 800 S m^{-1}. This optimized rGO-MoS_2 composite electrode exhibited an approximate 11 % reduction in sheet resistance compared to the unoptimized composite. Furthermore, all samples show an improvement in sheet resistance values compared to pure rGO and MoS_2, which were 82.5 Ω/sq and 48.9 Ω/sq. Numerical simulations further revealed a 13.23 % improvement in device performance when the optimized rGO-MoS_2 composite was implemented as the top electrode in an inverted perovskite solar cell, demonstrating the significant potential of this material for various electronic applications.

1. Introduction

Perovskite solar cells (PSCs) hold immense potential for next-generation photovoltaic technology due to their high efficiency, tunable bandgap, and low-cost fabrication. However, a critical challenge hindering their widespread adoption is the reliance on expensive and potentially unstable metal electrodes for charge collection [1]. This introduction delves into the current state-of-the-art in carbon-based electrodes as a promising alternative to address these limitations. Metal electrodes like aluminium (Al), gold (Au), and silver (Ag) have been widely employed due to their favourable work functions and resistivities [2]. Additionally, their high cost and susceptibility to corrosion with the underlying perovskite layer hinder large-scale production and device stability. Additionally, the vacuum thermal evaporation technique used for metal deposition is expensive and energy-intensive [3].

Carbon presents itself as a compelling alternative due to its inherent advantages: affordability, chemical stability, excellent conductivity, and adaptability [4,5]. Carbon-based electrodes have demonstrated enhanced stability in perovskite solar cells compared to their metallic counterparts. For instance, Bogachuk et al. have reported that perovskite solar cells with carbon-based top electrodes demonstrate superior corrosion resistance compared to those with metallic electrodes [6]. Additionally, the hydrophobic nature of carbon protects the underlying

* Corresponding author: Fakulti Teknologi Dan Kejuruteraan Industri Dan Pembuatan, Universiti Teknikal Malaysia Melaka, Hang Tuah Jaya, 76100, Durian Tunggal, Melaka, Malaysia.
E-mail address: asyadi@utem.edu.my (M.A. Azam).

https://doi.org/10.1016/j.rineng.2024.102237
Received 3 December 2023; Received in revised form 29 April 2024; Accepted 6 May 2024
Available online 8 May 2024

layers from moisture-induced degradation [7]. The energy level of carbon-based materials is similar to that of Au, which makes them a promising candidate for top electrode materials [8]. Nevertheless, the performance of carbon-based perovskite solar cells still lags behind that of metallic electrodes due to insufficient charge-selective properties of the carbon electrode and interfacial charge recombination between perovskite/carbon, electron transport layer (ETL)/carbon, or hole transport layer (HTL)/carbon, depending on the device architecture employed [9].

Recent advancements in graphene-based electrodes offer promising solutions. Graphene is a valuable carbon material due to its exceptional charge mobility, conductivity, mechanical strength, large surface area, and non-reactivity to halides [10]. A study by O'Sullivan et al. found that CVD-2D graphene exhibits the capability to serve as a flexible, transfer-free, and transparent electrode, potentially replacing the conventional indium tin oxide (ITO) electrode in inverted perovskite solar cells (p-i-n) [11,12]. Nonetheless, if intended for use as a top electrode, reduced graphene oxide (rGO) in the form of 3D graphene appears to be a more fitting and economical alternative to CVD-2D graphene. For instance, a composite electrode from Ni-doped graphene (Ni-NG) has been explored by Guo et al. positively reducing graphene's work function. Decreasing the work function of the graphene is critical to enhancing the efficiency of the hole extraction process at the perovskite/electrode interface. The Ni-NG achieved a champion power conversion efficiency (PCE) of 12.39 % [13]. According to recent research in 2021 by Mariani et al. using a graphene-doped carbon electrode as a hole collector in perovskite solar cells resulted in a power conversion efficiency of 15.81 % and improved thermal stability compared to an Au electrode [14]. Additionally, this work reported that the carbon electrode exhibited a sheet resistance value of around 17 Ω sq^{-1} for a 40 μm thickness. Incorporating graphene flakes into the carbon electrode helped slow charge thermalization processes and improved hot-carrier extraction and collection [15].

This work focuses on the potential of rGO-MoS_2 composites for top electrodes in p-i-n perovskite solar cells. MoS_2, with its exceptional mechanical and electrical properties, combined with the high surface area and conductivity of rGO, offers an exciting opportunity to create an electrode with enhanced mechanical strength, electrical conductivity, and thermal stability [16,17]. The unique layered structure of MoS_2 and the high surface area of rGO could also lead to improved interfacial bonding and enhanced interactions within the composite [18]. While graphene-based top electrodes have been explored for hole collection in n-i-p architectures, their potential as electron collectors in p-i-n architectures remains largely unexplored. This study investigates the feasibility of using an rGO-MoS_2 composite electrode as an electron collector in p-i-n perovskite solar cells. We explore the composite's ability to provide a conductive pathway for electron movement and its tunability to match the energy level of the perovskite material, potentially leading to increased charge transportation efficiency. To optimize the electrical conductivity of the rGO-MoS_2 composite electrode, a statistical analysis approach, namely Taguchi's design, is employed. This robust method allows for the identification of the most significant factors and their interactions, enabling the systematic optimization of the composite's properties for enhanced electrical performance. The novelty of this study lies in the systematic optimization of the rGO-MoS2 composite electrode fabrication using the Taguchi method, a robust statistical approach that allowed us to identify the most significant factors and their optimal levels for maximizing the electrical conductivity.

2. Methodology

2.1. Synthesis of rGO-MoS_2 composite

The composite of reduced graphene oxide (rGO) and molybdenum disulfide (MoS_2, Sigma Aldrich, USA) is made through a one-pot hydrothermal process. Initially, the rGO powder is synthesized via low-temperature top-down modified Hummer's method from graphite as the starting material. The reducing agent used is non-toxic, which is ascorbic acid. The detailed step to synthesise the rGO is based on our previous work [19]. For the rGO-MoS_2 composite, briefly, the rGO powder and MoS_2 powder are added to 30 mL of deionized water and subjected to 2 h of sonication. The mixture is then transferred to an autoclave and heated at a temperature of 180 °C for 12 h in the furnace. After this step, the rGO-MoS_2 suspension is centrifuged at 3500 rpm for 10 min to remove the presence of the supernatant. To further purify the precipitate, 100 mL of 1 M hydrochloric acid (HCl, R&M Chemicals, USA) is added, and the solution is centrifuged under the same conditions for another 10 min. This washing process is repeated several times with deionized water. The last step involves removing the supernatant and drying the precipitate in the oven at 60 °C for 1 h. Finally, the precipitate is ground to produce a fine powder of the rGO-MoS_2 composite. Three weight ratios were selected to investigate the effect of varying rGO and MoS_2 content on the composite electrode's properties: 1:3 (higher content of MoS_2), 1:1 (balanced), and 3:1 (higher content of rGO). This allows for a comprehensive evaluation of the composite's performance and electrical conductivity as a function of the relative concentrations of the two components.

2.2. Preparation of rGO-MoS_2 electrode slurry

In this particular study, a slurry electrode was produced utilizing the ball milling technique. The electrode was composed of 10 wt% polymethyl methacrylate (PMMA, Sigma Aldrich, USA) as a binder and 80 wt % of a mixture of rGO-MoS_2 as the active material (AM), along with 10 wt% acetylene black (AB, Sanji Chemical, China), which served as a carbon-conductive filler. To dissolve the AM, 10 mL of chlorobenzene (CB, R&M Chemicals, USA) was used as the solvent for every 1 g of AM. The mixture was then ball milled at a rate of 300 rpm for 6 h. The resulting slurry was carefully stored in a glass bottle and hermetically sealed to prevent drying out.

2.3. Design of experiment via taguchi technique for preparation of electrode film

The rGO-MoS_2 electrode-thin film was prepared from the slurry (described in subsection 2.2) using the doctor-blading technique. After depositing the slurry on the substrate and allowing it to fully dry, the electrical conductivity of the film was evaluated. All the processes are summarized in Fig. 1. Analyzing the conductivity of rGO-MoS_2 composite offers a powerful tool for assessing both the quality of material synthesis and the degree of composite formation. Increased conductivity typically corresponds to improved electron transport. A decrease in conductivity could be symptomatic of a range of issues, such as incomplete reduction of graphene oxide or inadequate dispersion of MoS_2 within the composite, all of which could hinder device performance. To ensure optimal results, the Taguchi design was employed as a reliable tool for the Design of Experiments (DOE) during the preparation of the rGO-MoS_2 composite electrode from the prepared slurry. The statistical method was used to analyze the outcomes and determine the best combination of control factors, such as the weight ratio of the active material (AM), which is rGO and MoS_2, heating temperature, and heating period. Each of these control factors is classified into three levels as summarized in Table 1. The three different weight ratios of the AM (A) were prepared during slurry preparation while the heating temperature (B), and heating period (C) were measured using a hot plate and stopwatch during the drying process after the slurry electrode was deposited on the substrate. The sheet resistance of the electrode film was measured to assess the output response, considering the relative humidity of the environment, which was divided into two levels: above (U1) and below (U2) 80 % relative humidity (RH), to account for the environmental factor's impact on the results. The sheet resistance of the rGO-MoS_2 electrode thin film was examined by using a four-point probe

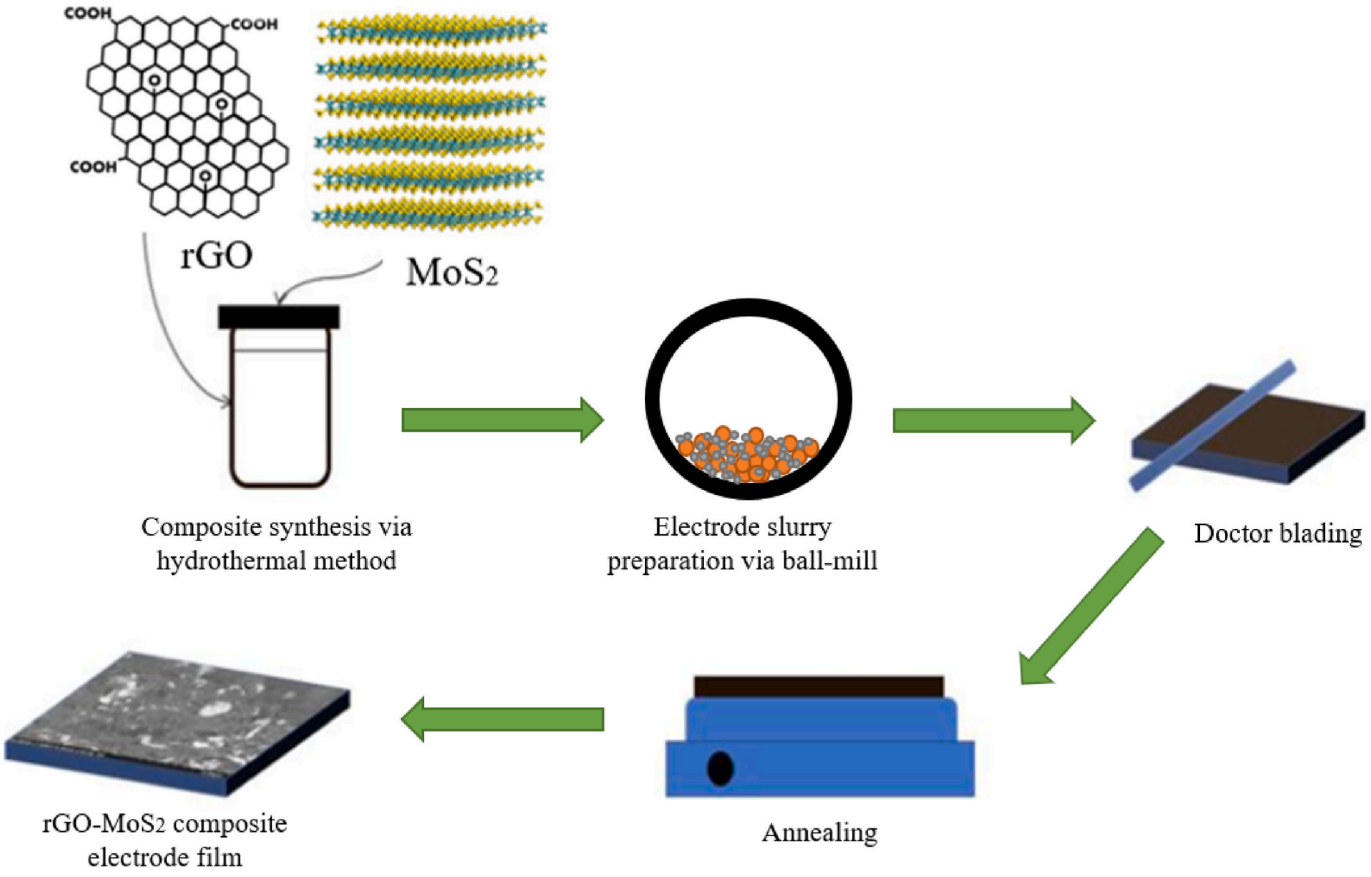

Fig. 1. Procedure to prepare the rGO-MoS_2 composite electrode thin film.

Table 1
Sheet resistance value for rGO-MoS_2 composite electrode film measured in L9 OA.

Experiment number	Control factors			Average sheet resistance (Ω/sq)	Noise	
	A	B (°C)	C (min)		U1 (Ω/sq)	U2 (Ω/sq)
1	1:1	30	5	10.16 ± 0.02	10.14	10.18
2	1:3	120	5	9.74 ± 0.02	9.72	9.75
3	3:1	120	10	11.03 ± 0.05	10.49	11.56
4	3:1	30	15	9.70 ± 0.01	9.69	9.70
5	3:1	75	5	10.16 ± 0.04	10.12	10.19
6	1:1	75	10	9.68 ± 0.07	9.61	9.74
7	1:1	120	15	9.98 ± 0.01	9.97	9.98
8	1:3	30	10	10.46 ± 0.04	10.42	10.49
9	1:3	75	15	9.82 ± 0.02	9.83	9.8

Table 2
Result of ANOVA and the best setting of control factors.

Symbol	Control factor	Units	Level	Best Value	Factor effect, FE (%)
A	Ratio of AM	–	1	1:1	13 (significant)
B	Heating temperature	°C	2	75	13 (significant)
C	Heating period	Minutes	3	15	30 (dominant)

analysis as the output response. Furthermore, various materials analysis techniques, such as Raman, XRD, and FESEM, were employed to characterize the rGO-MoS_2 electrode. Solar cell capacitance simulator (SCAPS-1D) software (version 3.3.10) was utilized to simulate the performance of the PSC device, which helped verify the suitability of the rGO-MoS_2 composite electrode for use in perovskite solar cells (PSCs)

3. Results and discussion

The Taguchi optimization approach was employed to systematically investigate the fabrication of rGO-MoS_2 composite electrodes for inverted perovskite solar cells. The L_9 orthogonal array was used to conduct nine experimental runs, and the signal-to-noise ratio (SNR) was calculated to identify the optimal combination of control factors that minimized the sheet resistance. Taguchi orthogonal arrays are a powerful tool for systematically organizing parameters, helping determine optimal levels and facilitate experimental design. They account for pair-wise interactions, provide comprehensive information, and yield speedy results. In this study, nine experimental runs were conducted using the L9 orthogonal array (OA) of the Taguchi design. The L9 orthogonal array (OA) is a balanced design chosen for its efficiency. It minimizes the number of experiments required while providing adequate information about different process parameters, particularly when dealing with 3-level control factors. The aim was to obtain a minimize sheet resistance and optimize the Taguchi signal-to-noise ratio (SNR) for the 'smaller-the-better' characteristics, ηs which is calculated by the following equation.

$$\eta s = -10 \log \left(\frac{1}{n \sum_{i=1}^{n} y_i^2} \right) \quad (1)$$

Where, the value of the ith experiment in each group is represented by y, while n is the number of experiments.

The results of these experiments are summarized in Table 1. The means of SNR were then computed to identify which levels had the most significant influence on every control factor via analysis of variance

(ANOVA). Fig. 2 shows the main effects plot of the signal-to-noise (SN), with the higher percentage of levels selected and combined as the best setting for a confirmatory test that is found to be insensitive to noise factors. The ANOVA and factor effect (FE) analysis provided deeper insights into the influence of the three control factors on the sheet resistance of the rGO-MoS_2 composite electrodes, as shown in Table 2. The ANOVA and factor effect (FE) analysis revealed that the heating period (factor C) had the most significant influence, contributing 30 % to the sheet resistance value. This was mainly driven by the longest heating duration (15 min, level C3), which facilitated efficient drying and improved the interconnectivity of the rGO and MoS_2 components within the composite film.

The active material (AM) ratio (factor A, 13 % FE) and heating temperature (factor B, 13 % FE) also showed substantial effects on the sheet resistance. The 1:1 rGO-MoS_2 ratio (A1) yielded the optimal results, indicating that this composition provided the best balance between the contributions of rGO and MoS_2 to the overall electrical conductivity of the composite. The 75 °C heating temperature (B2) was found to be the optimal level, as it likely promoted the interfacial interactions between the rGO and MoS_2 components. Therefore, the best combination of factors to obtain a low sheet resistance electrode is found to be A1B2C3. The synergistic effects of the rGO and MoS_2 components within the composite were a key factor in the improved electrical conductivity compared to the pure rGO and MoS_2 films. The rGO provided a highly conductive network that facilitated electron transport, while the MoS_2 nanosheets enhanced the overall charge carrier mobility within the composite structure.

To validate the findings from the Taguchi analysis, a confirmation test was performed by applying the A1B2C3 selected as the optimal level to fabricate the rGO-MoS_2 electrode thin film. From the Taguchi analysis, the predicted value of sheet resistance on optimization ranges from 9.42 Ω/sq to 9.61 Ω/sq, while the mean is 9.51 Ω/sq (see supplementary). Three samples of rGO-MoS_2 electrode thin film were fabricated using the A1B2C3 parameters. The measured mean sheet resistance was 9.46 ± 0.01 Ω/sq, shown in Table 3, this value falls within the predicted range and is lower than the average predicted value. This improvement can be attributed to the favourable interactions between the rGO and MoS_2 components, as well as the efficient drying and interconnectivity achieved under the optimized fabrication conditions. The result obtained is more favourable for this hydrothermal rGO-MoS_2 composite as compared to our previous study which used a stirring process [20]. Furthermore, all samples show an improvement in sheet resistance values compared to pure rGO and MoS_2, which were 82.5 Ω/sq and 48.9 Ω/sq. The comprehensive DOE analysis, including ANOVA and factor effect evaluation, provided valuable insights into the complex interplay between the various control factors and their impact on the electrical properties of the rGO-MoS_2 composite electrodes. This systematic approach allowed for the identification of the most influential parameters and their optimal levels, leading to the development of highly conductive composite electrodes that are well-suited for use in electronic and electrical applications.

Electrical conductivity is one of the essential properties to consider when selecting an electrode as a current collector, which provides information about the ability of electrons to flow easily through it [21,22]. The electrical conductivity, σ of the rGO-MoS_2 electrode fabricated in this work was calculated, using the sheet resistance (Rsh) measured using a four-point probe and the electrode film thickness (t) measured from the FESEM image in Fig. 3.

$$\sigma = 1 / (R_{sh} \times t) \quad (2)$$

Table 3
Sheet resistance value upon confirmation test.

After optimization	Sheet resistance 1 (Ω/sq)	Sheet resistance 2 (Ω/sq)	Sheet resistance 3 (Ω/sq)	Average sheet resistance (Ω/sq)
A1B2C3	9.46	9.45	9.46	9.46 ± 0.01

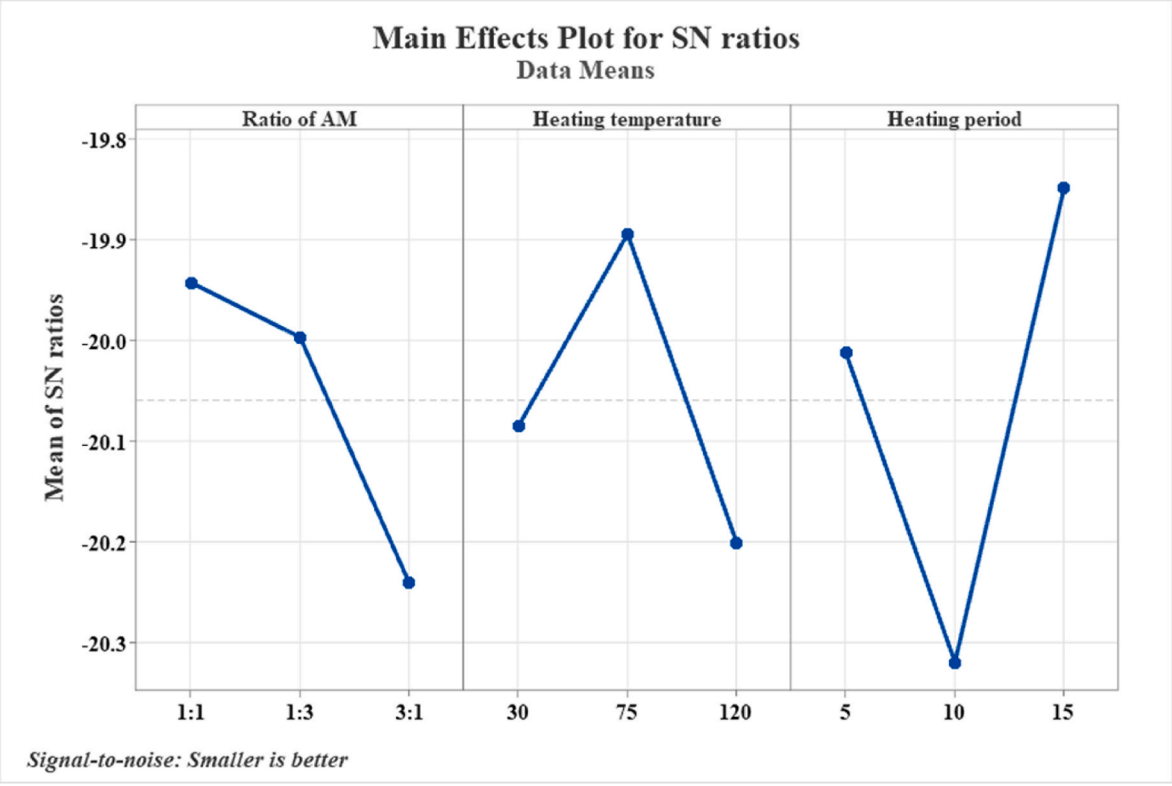

Fig. 2. Main effect plot of the SN ratios for the output response, sheet resistance for rGO- MoS_2 electrode.

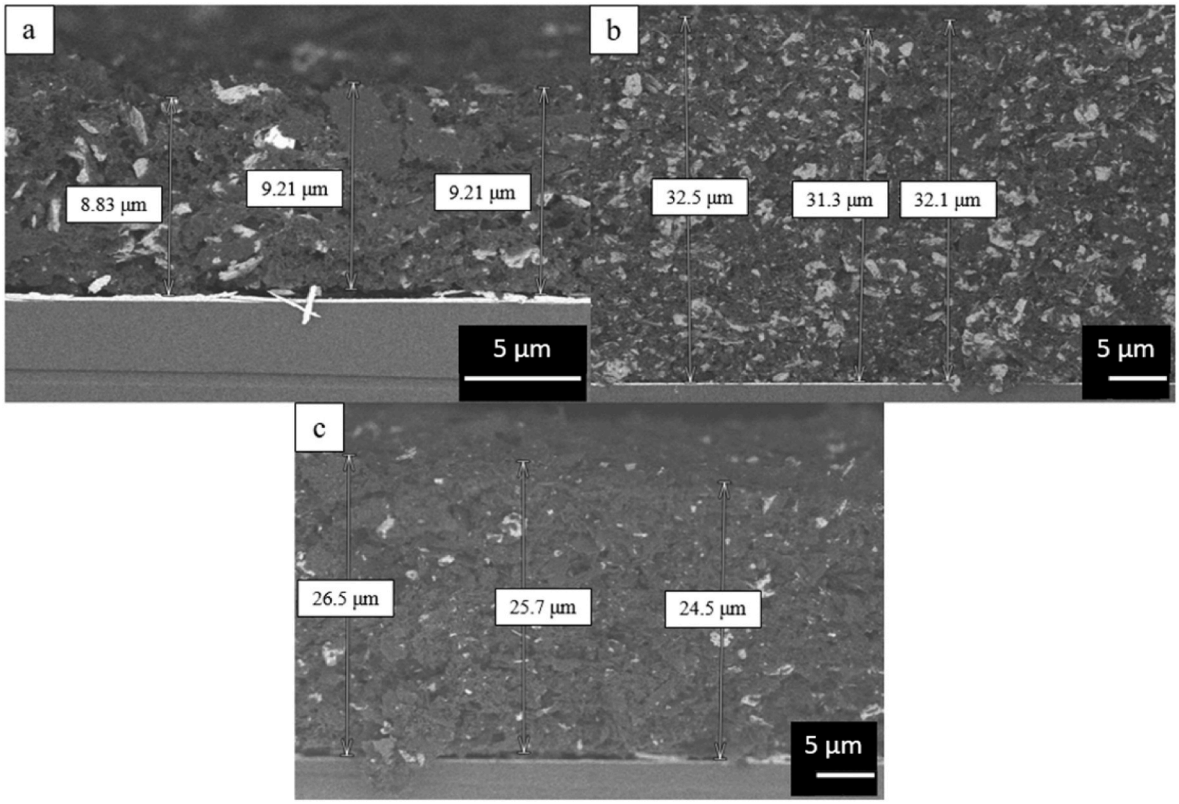

Fig. 3. (a–c) Back-scattered FESEM image of cross-sectional thickness for rGO-MoS_2 composite electrode thin film at three different spots.

The calculated electrical conductivities for rGO-MoS_2composite electrode films with different ratios are summarized in Table 4 rGO-MoS_2 (1:1) exhibited the highest electrical conductivity. This is attributed to its narrow optical bandgap (details in supplementary) and thin cross-sectional thickness. This property makes it a promising candidate for the top electrode in p-i-n perovskite solar cells. Reduced electrode thickness shortens the travel distance for charge carriers, leading to more efficient charge extraction [23]. Additionally, thinner electrodes can minimize charge carrier recombination, further enhancing overall solar cell efficiency [24]. This property makes the rGO-MoS_2 (1:1) composite a promising candidate for the top electrode in p-i-n perovskite solar cells.

The higher electrical conductivity of the rGO-MoS_2 composite electrode is attributed to the rGO nanosheets' structure facilitates charge carrier transport through the MoS_2 matrix, lowering the interfacial energy barrier [25]. The structural and morphological properties of the rGO-MoS_2 composite were studied using FESEM to observe the effects of adding MoS_2. Fig. 4 shows the FESEM image of the rGO-MoS2 (1:1) electrode cross-section on ITO glass at two magnifications for comparison. Image (a) is a backscatter electron image of (b). In the backscattered image, MoS_2 appears brighter than rGO due to its higher atomic weight. The FESEM images clearly show that MoS_2 is well distributed throughout the rGO-MoS_2 composite electrode. The close-up images (c) and (d) reveal that it can be seen that the MoS_2 layers are interspersed between the rGO sheets, while the ball-like carbon black acts as a conductive filler, bridging the gaps and promoting electron transport within the composite electrode [26]. Also, EDX elemental mapping analysis, shown in Fig. 5 confirms the distribution of elements C and O from the rGO and carbon conductive filler, meanwhile, elements Mo and S are from MoS_2 throughout the rGO-MoS_2 composite electrode. The rGO nanosheets provide a highly conductive network that facilitates efficient charge transport through the MoS_2 matrix, as evidenced by the FESEM images. The intimate contact between the rGO and MoS_2 layers, as well as the presence of conductive carbon black filler, creates an interconnected network of conductive pathways that enhances the overall electrical conductivity of the composite. This is further supported by the Raman spectroscopy analysis, which revealed a blue shift in the characteristic peaks, indicating improved coupling and effective bond strength between the graphene and MoS_2 layers.

Table 4
Electrical conductivity value for rGO-MoS_2 electrode thin film.

Sample	Average thickness, tavg ($\times 10^{-6}$ m)	Average sheet resistance, (Ω/sq)	Electrical conductivity, σ (S m^{-1})
RM 1:1	9.08	9.46	11800.00
RM 1:3	31.97	9.74	3211.43
RM 3:1	25.57	9.70	4031.79
Pure rGO	9.33	82.5	1300.00
Pure MoS_2	10.26	48.9	1990.00

Fig. 6 (a) displays the Raman spectra of the rGO-MoS_2 composite at different weight ratios. The Raman spectra of rGO exhibit two peaks at around 1342 cm-1 and 1576 cm-1, indicating the D-band and G-band, respectively. These peaks represent the vibration of sp2-bonded carbon atoms and defect-induced vibration. Conversely, the MoS_2 displays two distinct peaks at 372 cm-1 and 400 cm-1, which represent the in-plane (E^1_{2g}) and out-of-plane (A_{1g}) modes. The composite displays four distinct peaks, representing the D and G bands of pure rGO, and E^1_{2g} and A_{1g} of pure MoS_2, for all samples. This confirms the rGO-MoS_2 coupling, as reported elsewhere [27]. Although the intensity of the D and G bands of rGO remains consistent across all ratios of rGO-MoS_2 composites, the intensity of E^1_{2g} and A_{1g} decreases as the proportion of MoS_2 in the composite decreases. This trend reflects the varying MoS_2 content in the composites. The Raman analysis reveals a blue shift of the E^1_{2g} and A_{1g} peak positions compared to pristine MoS_2 (see supplementary). This

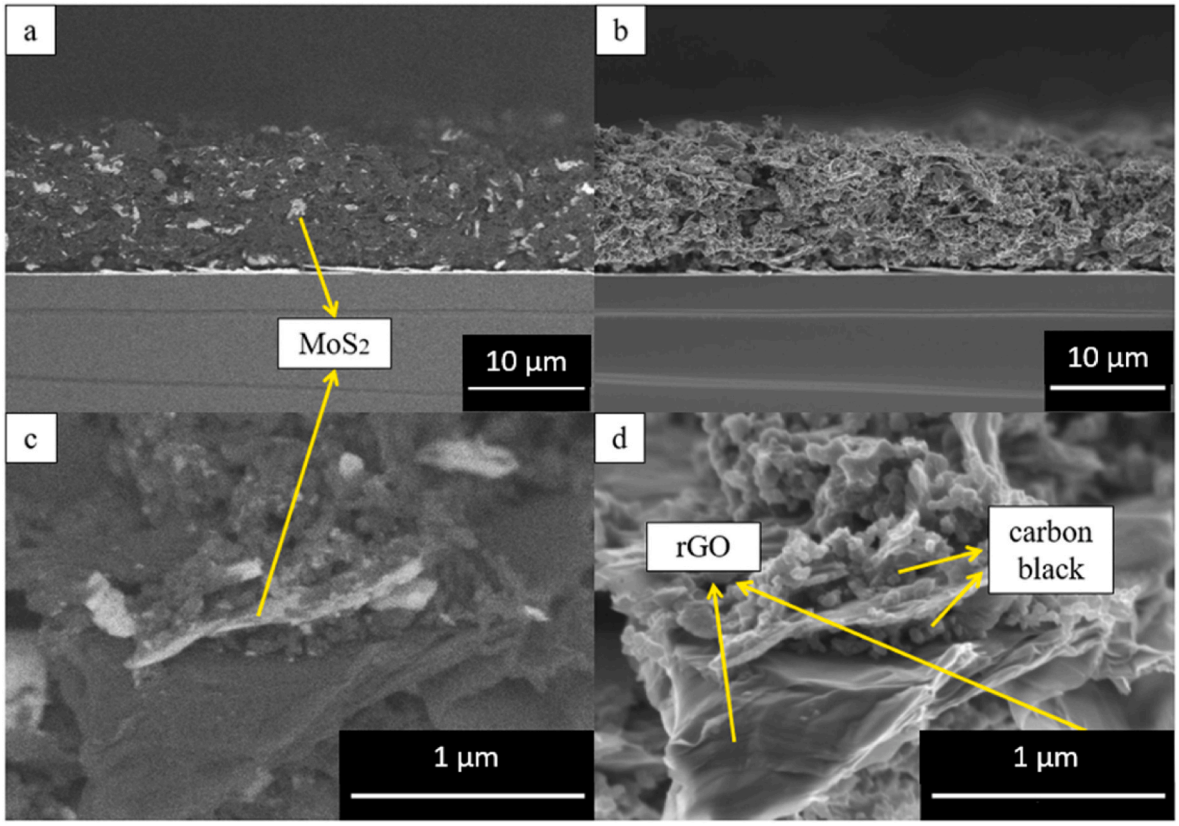

Fig. 4. (a and c) Backscattered FESEM image at 10 µm and 1 µm scale bars, (b and d) FESEM image at 10 µm and 1 µm scale bars for cross-section of a rGO-MoS_2 (1:1) composite electrode fabricated on ITO glass.

shift indicates an increase in the frequency or wavenumber of phonons interacting with the photon. Similarly, the D and G bands exhibit a blue shift, suggesting enhanced bond strength due to improved rGO-MoS_2 coupling (see supplementary), which suggests an enhancement in the effective bond strength due to improved coupling between the graphene and MoS_2 layers. These findings validate the successful formation of a composite from rGO and MoS_2.

An analysis using X-ray diffraction (XRD) was performed to examine the crystal structure of the examined samples. Fig. 6 (b) shows the XRD patterns of the rGO, MoS_2, and rGO-MoS_2 composites. The rGO patterns display a broad peak at $2\theta = 24.31°$, corresponding to the (002) plane observed in the XRD patterns of rGO, consistent with previous findings reported by Chen et al. [28]. The pure MoS_2 exhibited peaks at 14.2°, 28.86°, 32.9°, 33.5°, 35.9°, 39.7°, 44.03°, 49.8°, 59.7°, and 60.2°, corresponding to (002), (004), (100), (101), (102), (103), (006), (105), (110), and (008) planes, respectively, as per (JCPDS No. 06–0097). All rGO-MoS_2 composite patterns contain peaks for both rGO and MoS_2. The 2H MoS_2 peak, located at $2\theta = 14.2°$, signifies the semiconductor properties of the MoS_2. This phase is more stable and less resistant to oxidation than the 1T-phase [29]. The 2H phase is preferred for rGO composites due to its superior stability and durability, ensuring electrode film integrity.

The rGO-MoS_2 (3:1) composite exhibits a stronger (002) orientation due to its higher rGO content. This suggests that higher rGO content in the rGO-MoS_2 composite leads to a stronger (002) peak, suggesting a more prominent rGO presence. Meanwhile, peaks in the (103) and (008) planes weaken, indicating reduced MoS_2 presence. Additionally, the (004) peak is notably absent. According to research by Rasamani et al. this can lead to MoS_2 layer inhibition by rGO nanosheets, resulting in reduced MoS_2 content through rearrangement [30]. In contrast, the (1:3) sample shows more prominent MoS_2 peaks. However, sample (1:1), which contains the same weight percent ratio of rGO and MoS_2, lacks the broad (002) peak of rGO. However, a faint peak suggests increased crystallinity of the rGO structure in the (1:1) composite. This aligns with the earlier Raman results, supporting the progressive formation of the rGO-MoS_2 composite. At a 1:1 ratio, the structural behaviour of rGO in conjunction with MoS_2 may deviate from the typical stacking pattern along the (002) plane, potentially due to interactions with MoS_2 layers or the formation of unique nanostructures/interfaces within the composite. This alteration could lead to the absence of a distinct (002) peak for rGO in the composite. This scientific insight aligns with findings on the influence of MoS_2 on the structural properties of nanomaterial composites [31]. The interplay between rGO and MoS_2 at specific ratios can induce structural modifications that impact the stacking arrangement of rGO nanosheets, elucidating the absence of the characteristic (002) peak in the (1:1) composite [32].

This study demonstrates the potential of rGO-MoS_2 composite as the top electrode in the inverted perovskite solar cell with ITO/CuSCN/MAPbI3/PCBM/BCP/rGO-MoS_2 architecture. The device performance was simulated using Solar Cell Capacitance Simulator (SCAPS) – 1D software, where the numerical details are explained in supplementary. Simulation analysis allowed for flexibility to explore diverse scenarios and test hypotheses. Details on the simulation parameters can be found in Table 5, which were compiled from previous literature [33–35] except for the rGO-MoS_2 thickness and bandgap, determined experimentally. The program was conducted with an illuminance of 1000 W/m^2. The following values of characteristic energy (0.1 eV), thermal velocity of charges (1×10^7 cm/s), Gaussian defect distribution, ETL and HTL defects located at the centre of the interface gap, are considered independently of each layer type. Fig. 7 reveals the significantly different I–V curve characteristics of a device with a silver electrode compared to the rGO-MoS_2 electrode. Replacing the silver electrode with the rGO-MoS_2 composite significantly increased the fill factor (FF) from 44.24 to 66.59. This resulted in a remarkable improvement in

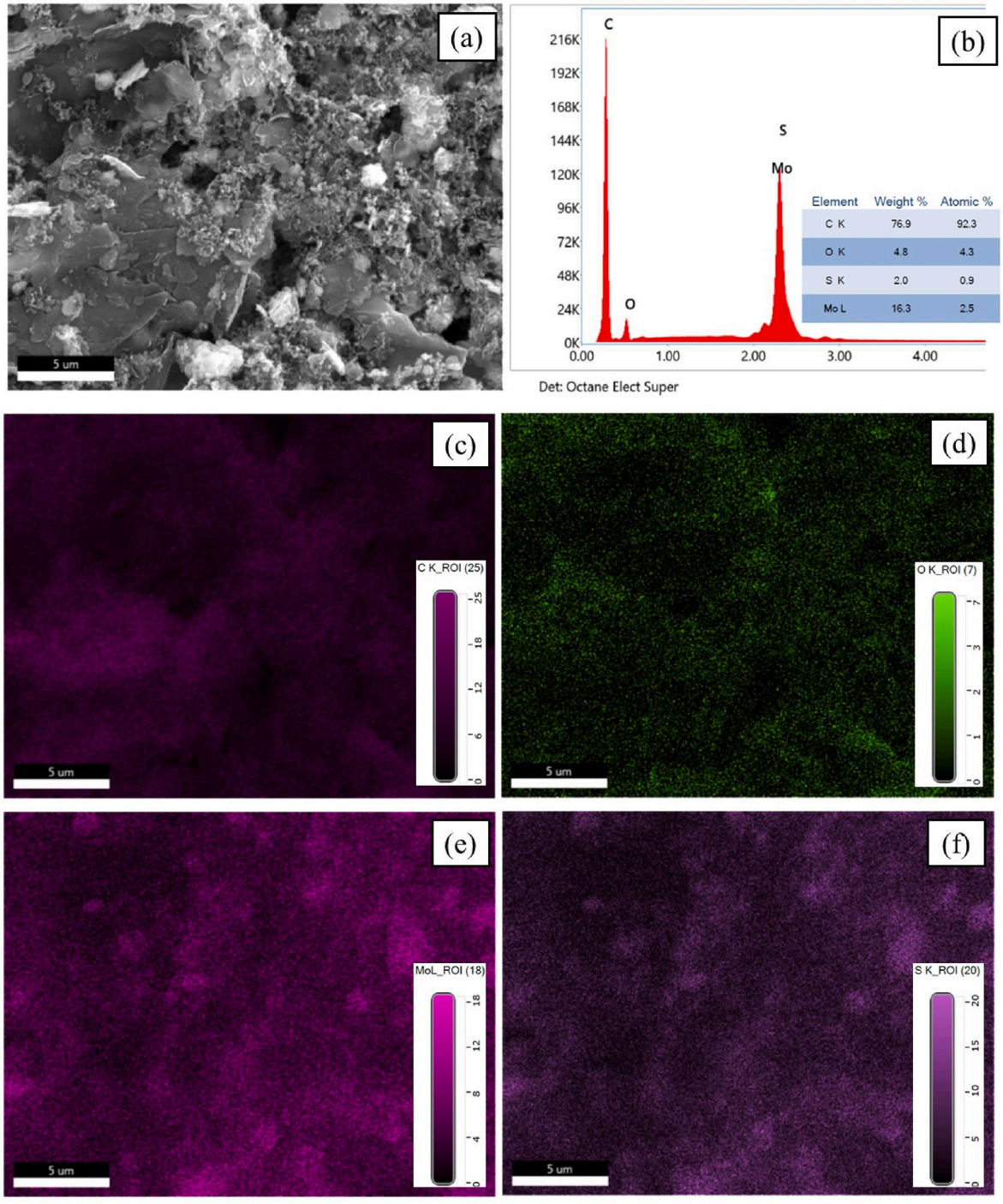

Fig. 5. (a) SEM image, (b) EDX analysis, (c–f) Elemental mapping analysis of rGO-MoS_2 (1:1) composite electrode.

power conversion efficiency (PCE) from 10.37 % to 13.23 % (refer to Table 6). These findings suggest that the rGO-MoS_2 composite electrode serves as an effective current collector that suits the inverted device configuration.

The rGO-MoS_2 composite offers numerous advantages due to the strong interaction between the delocalized π-electrons of rGO and the outer electrons of S atoms in MoS_2 [36]. This interaction forms an electron-rich zone between S atoms and rGO, enabling efficient charge transport across the composite [37]. The intimate contact between rGO and MoS_2, evident in FESEM images (Fig. 4), fosters strong synergistic interactions and a consequent boost in electrical conductivity. Beyond photovoltaic applications, these composite holds promise for sensors [38], energy storage [39], and even high-performance structural materials [40]. Fig. 8 (a) shows the optimal parameter for rGO-MoS_2 electrode fabrication. Fig. 8 (b) visually depicts the interconnected network of conductive pathways resulting from the close contact between rGO and MoS_2, which enhances the overall electrical conductivity of the composite. Table 7 compares the sheet resistance and conductivity of the rGO-MoS_2 composite electrode with a conventional carbon electrode from the literature. Lower sheet resistance yields the promising conductivity obtained for the rGO-MoS_2 composite prepared in this work, as a promising electrode material for high-performance perovskite solar cells. The superior electrical conductivity of the rGO-MoS_2 composite (11 800 S m^{-1} for the 1:1 ratio) compared to conventional carbon

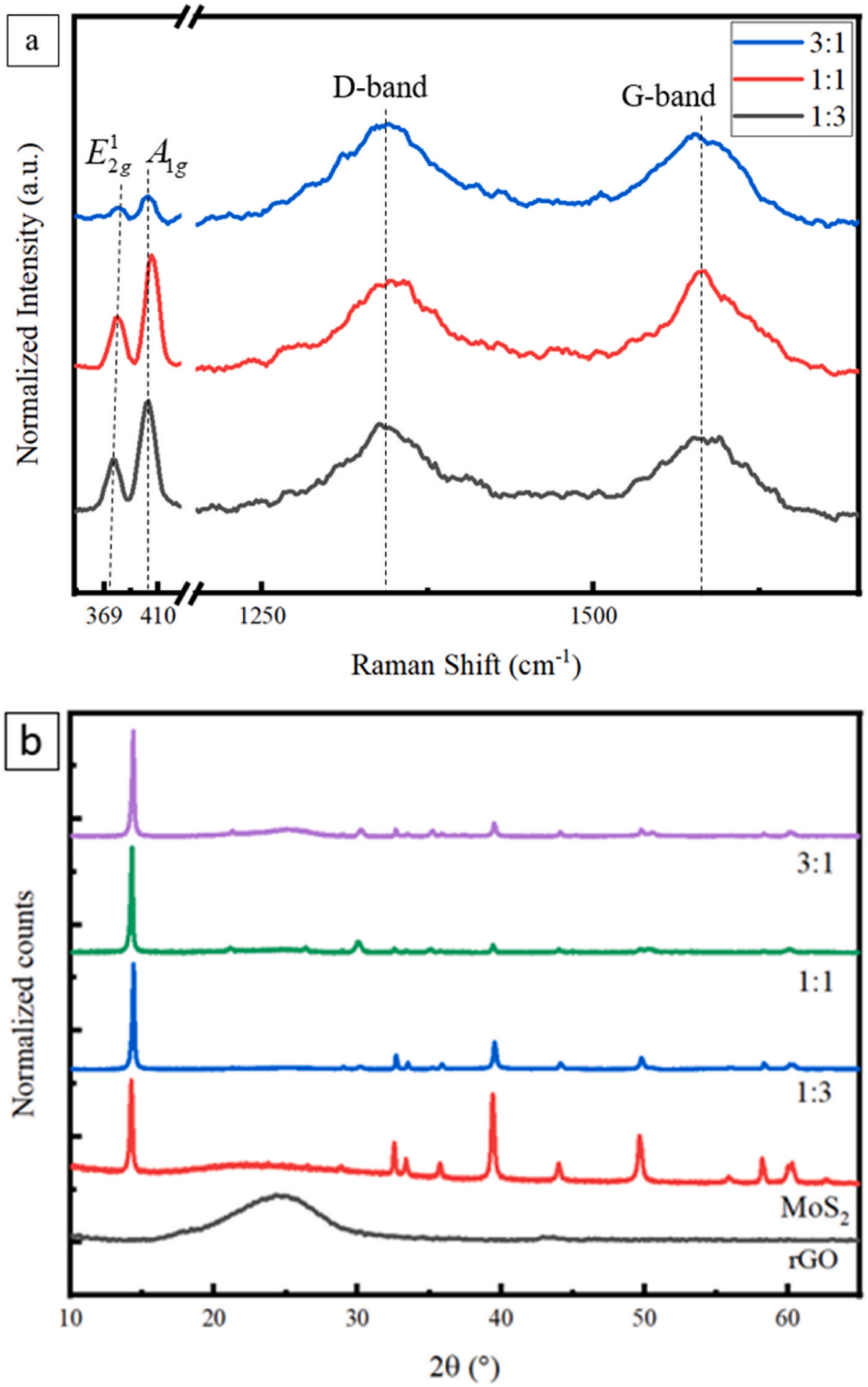

Fig. 6. (a) Raman spectra of rGO-MoS_2 composites electrode (b) XRD patterns for all examined samples.

electrodes can be attributed to the synergistic interactions between the rGO and MoS_2 components. The delocalized π-electrons of rGO interact with the outer electrons of sulfur atoms in MoS_2, forming an electron-rich zone that enables efficient charge transport across the composite. Additionally, the thin cross-sectional thickness of the rGO--MoS_2 (1:1) electrode reduces the travel distance for charge carriers, leading to more efficient charge extraction and minimizing recombination losses.

The entire research demonstrates the effective use of the Taguchi method in optimizing the fabrication process of rGO-MoS_2 electrodes for inverted perovskite solar cells. The optimized parameters led to an improvement in conductivity and simulated device performance, indicating its potential to enhance the efficiency of actual devices. The superior electrical conductivity of the rGO-MoS_2 composite (11 800 S m^{-1} for the 1:1 ratio) compared to conventional carbon electrodes can be attributed to the synergistic interactions between the rGO and MoS_2 components. This research highlights the Taguchi method as a systematic and effective technique for electrode optimization, which can accelerate advancements in various technologies through a structured and data-driven approach.

Table 5
Device Simulation parameter.

Parameters	CuSCN	srGO-MAPbI3	PCBM	BCP	rGO-MoS_2
t (nm)	24	283	92.1	51	9080
Eg (eV)	3.4	1.58	2	3.5	1.25
χ (eV)	1.9	3.9	4.2	3.7	4.5
εr (relative)	10	10	3.9	10	10
Nc ($1/cm^3$)	1.7×10^{19}	2.2×10^{18}	2.5×10^{21}	2.2×10^{18}	2.2×10^{19}
Nv ($1/cm^3$)	2.5×10^{21}	1×10^{19}	2.5×10^{21}	1.8×10^{18}	1.8×10^{18}
μe (cm^2/vs)	1×10^{-1}	2.2	2×10^{-1}	1×10^{7}	3.95×10^{2}
μh (cm^2/vs)	1×10^{-4}	2.2	2×10^{-1}	1×10^{7}	3.95×10^{2}
ND ($1/cm^3$)	0	1×10^{13}	2.93×10^{17}	1×10^{21}	1×10^{18}
NA ($1/cm^3$)	1×10^{18}	1×10^{12}	0	1×10^{10}	0

Band gap and thickness values were bold because the values were obtained from the experimental work in this study. Meanwhile, other parameters are taken from the results of the literature.

4. Conclusions

The Taguchi method was utilized in a study to optimize the fabrication process of rGO-MoS_2 electrodes for inverted perovskite solar cells. The study analyzed the impact of the rGO-MoS_2 mixing ratio, annealing temperature, and annealing time on the electrode's electrical conductivity. The optimal combination was found to be a 1:1 mixing ratio, 75 °C annealing temperature, and 15-min annealing time. This optimization strategy enhanced the electrical conductivity to 11 800 S m^{-1} compared to the non-optimized electrode. The morphological investigations suggested that the improvement resulted from the enhanced interaction between rGO and MoS_2, leading to superior charge transport within the electrode.

Simulations were conducted using SCAPS-1D to evaluate the potential of rGO-MoS_2 as a top electrode for inverted perovskite solar cells. The results showed that the device performance increased from 10.37 % (with Ag electrode) to 13.23 % with rGO-MoS_2. By substituting expensive gold and silver with rGO-MoS_2, a cost-effective alternative for inverted perovskite solar cells was offered. Additionally, the study highlighted the broader utility of the Taguchi method for optimizing electrode systems across diverse electronic devices, including photovoltaics, sensors, and energy storage devices. The work provides a systematic and efficient approach to electrode optimization and opens exciting opportunities for technological advancements.

CRediT authorship contribution statement

Nur Ezyanie Safie: Writing – review & editing, Writing – original draft, Visualization, Validation, Methodology, Investigation, Formal analysis, Data curation, Conceptualization. **Mohd Asyadi Azam:** Writing – review & editing, Supervision, Resources, Project administration, Conceptualization. **Faiz Arith:** Writing – review & editing, Formal analysis, Data curation. **T. Joseph Sahaya Anand:** Writing – review & editing. **Najmiah Radiah Mohamad:** Data curation. **Akito Takasaki:** Writing – review & editing.

Declaration of competing interest

The authors declare that they have no known competing financial

Table 6
Simulated device performance parameter for ITO/CuSCN/srGO-$MAPbI_3$/PCBM/BCP/Ag and ITO/CuSCN/srGO-$MAPbI_3$/PCBM/BCP/rGO-MoS_2.

Device	Jsc (mA/cm2)	Voc (V)	FF	PCE (%)
ITO/CuSCN/srGO-$MAPbI_3$/PCBM/BCP/Ag	19.929	1.177	44.24	10.37
ITO/CuSCN/srGO- $MAPbI_3$/PCBM/BCP/rGO-MoS_2	19.643	1.011	66.59	13.23

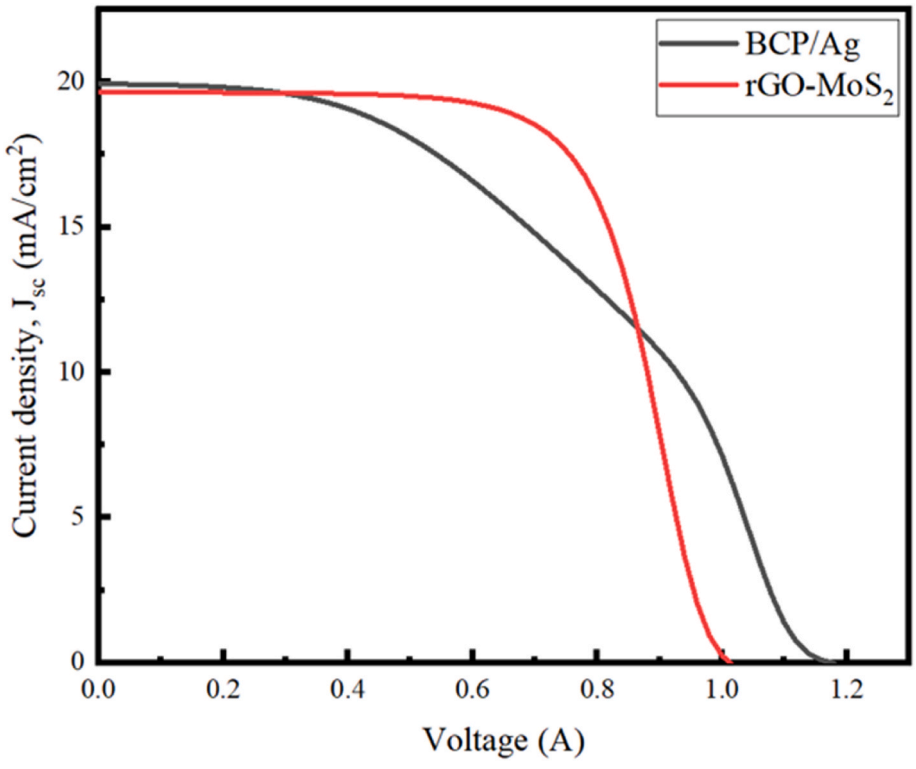

Fig. 7. Current-voltage characteristics of ITO/CuSCN/srGO-$MAPbI_3$/PCBM/BCP/Ag and ITO/CuSCN/srGO-$MAPbI_3$/PCBM/BCP/rGO-MoS_2.

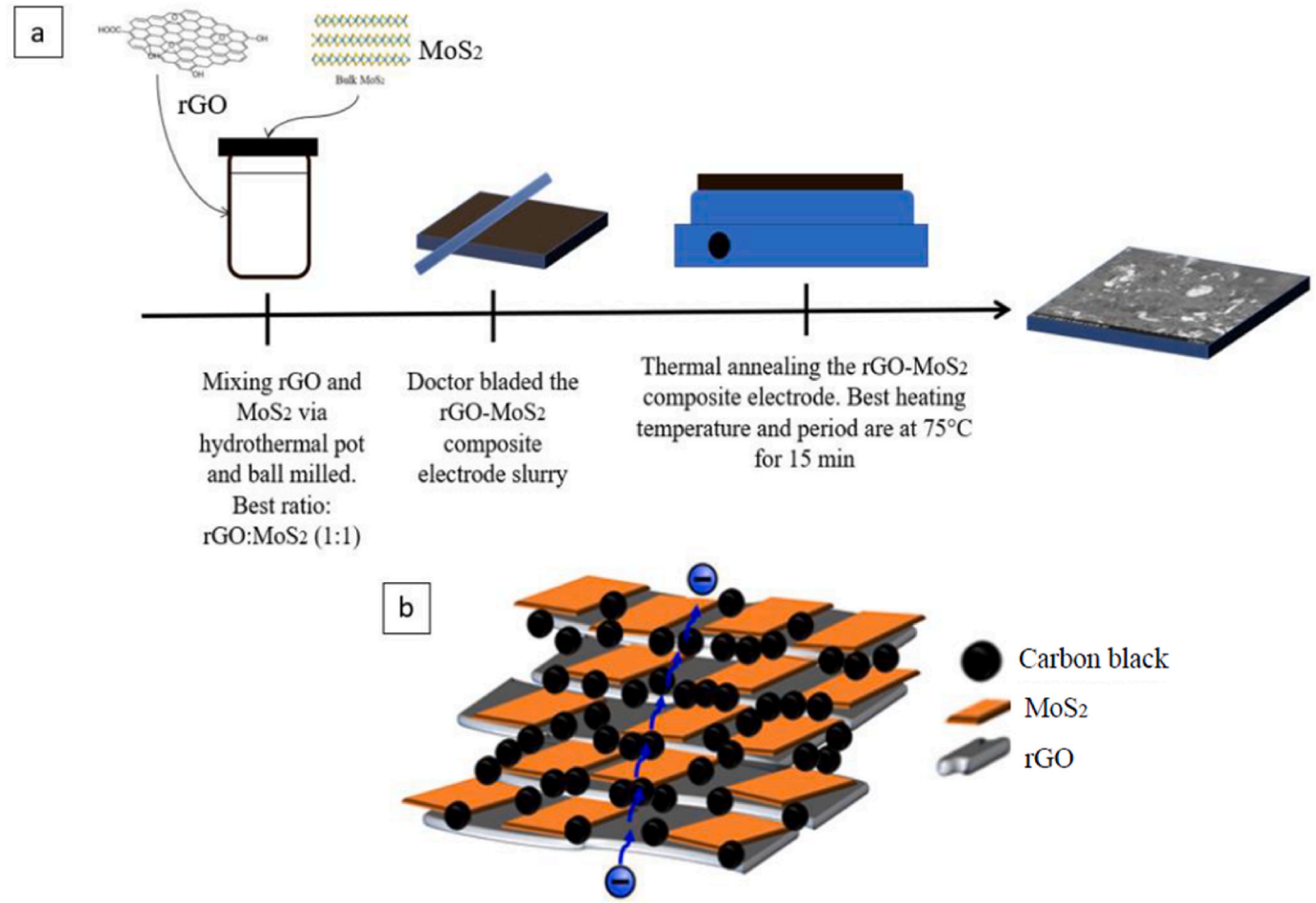

Fig. 8. (a) Optimal parameter to manufacture rGO-MoS_2 composite electrode. (b) Illustration of the interconnected network of conductive pathways for rGO-MoS_2 composite electrode.

Table 7
Comparison of the sheet resistance value obtained in this work with literature.

Main composition	Deposition method	Sheet resistance (Ω/sq)	Electrical conductivity, σ (S m-1)	Reference
Graphite, super P, ZrO_2	Screen printing	22.00	N/A	[41]
Graphite and carbon black	Doctor blading	20.50	1630	[42]
Graphene and carbon paste	Doctor blading	17.00	1470	[14]
rGO-MoS_2 composite and super P	Doctor blading	10.70	193	[20]
Cr and carbon	Screen printing	10.00	N/A	[43]
rGO-MoS_2 composite and acetylene black	Doctor blading	9.46	11800	This work

interests or personal relationships that could have appeared to influence the work reported in this paper.

Data availability

Data will be made available on request.

Acknowledgement

The authors are grateful to Universiti Teknikal Malaysia Melaka for the facilities support and to UTeM Zamalah Scheme for the PhD support of NE Safie.

Appendix A. Supplementary data

Supplementary data to this article can be found online at https://doi.org/10.1016/j.rineng.2024.102237.

References

[1] J. Wang, S.P. Senanayak, J. Liu, Y. Hu, Y. Shi, Z. Li, C. Zhang, B. Yang, L. Jiang, D. Di, A.V. Ievlev, Investigation of electrode electrochemical reactions in CH3NH3PbBr3 perovskite single-crystal field-effect transistors, Adv. Mater. 31 (2019) 1902618.
[2] D. Li, X. Dong, P. Cheng, L. Song, Z. Wu, Y. Chen, W. Huang, Metal halide perovskite/electrode contacts in charge-transporting-layer-free devices, Adv. Sci. 9 (2022) 2203683.
[3] M. Socol, N. Preda, G. Socol, Organic thin films deposited by matrix-assisted pulsed laser evaporation (MAPLE) for photovoltaic cell applications: a review, Coatings 11 (2021) 1368.
[4] S. Pandey, M. Karakoti, D. Bhardwaj, G. Tatrari, R. Sharma, L. Pandey, M.J. Lee, N. G. Sahoo, Recent advances in carbon-based materials for high-performance perovskite solar cells: gaps, challenges and fulfilment, Nanoscale Adv. 5 (2023) 1492–1526.
[5] M.R. Shekari, M. Golriz, S. Sadeghzadeh, Study of long-term stability of perovskite solar cells: highly stable carbon-based versus unstable gold-based PSCs, Journal of Renewable Energy and Environment 8 (2021) 61–73.

[6] D. Bogachuk, S. Zouhair, K. Wojciechowski, B. Yang, V. Babu, L. Wagner, B. Xu, J. Lim, S. Mastroianni, H. Pettersson, A. Hagfeldt, Low-temperature carbon-based electrodes in perovskite solar cells, Energy Environ. Sci. 13 (2020) 3880–3916.
[7] Z. Wu, Z. Liu, Z. Hu, Z. Hawash, L. Qiu, Y. Jiang, L.K. Ono, Y. Qi, Highly efficient and stable perovskite solar cells via modification of energy levels at the perovskite/carbon electrode interface, Adv. Mater. 31 (2019) 1804284.
[8] L.M. Gonzalez, D. Ramirez, F. Jaramillo, Current status and trends of carbon-based electrodes for fully solution-processed perovskite solar cells, J. Energy Chem. 68 (2022) 222–246.
[9] T. Yousaf, N. Shahzad, A. Sattar, M.A. Tariq, N. Hussain, Z.S. Khan, S. Javed, M. I. Shahzad, D. Pugliese, Performance of Cs-doped carbon-based perovskite solar cells in ambient environment, Energies 16 (2023) 4748.
[10] K. Gong, J. Hu, N. Cui, Y. Xue, L. Li, G. Long, S. Lin, The roles of graphene and its derivatives in perovskite solar cells: a review, Mater. Des. 211 (2021) 110170.
[11] V.D. Tran, S.V.N. Pammi, B.J. Park, Y. Han, C. Jeon, S.G. Yoon, Transfer-free graphene electrodes for super-flexible and semi-transparent perovskite solar cells fabricated under ambient air, Nano Energy 65 (2019) 104018.
[12] J. O'Sullivan, M. Wright, X. Niu, P. Miller, P.R. Wilshaw, R.S. Bonilla, Towards a graphene transparent conducting electrode for perovskite/silicon tandem solar cells, Prog. Photovoltaics Res. Appl. 31 (2023) 1478–1492.
[13] M. Guo, C. Wei, C. Liu, K. Zhang, H. Su, K. Xie, P. Zhai, J. Zhang, L. Liu, Composite electrode based on single-atom Ni doped graphene for planar carbon-based perovskite solar cells, Mater. Des. 209 (2021) 109972.
[14] P. Mariani, L. Najafi, G. Bianca, M.I. Zappia, L. Gabatel, A. Agresti, S. Pescetelli, A. Di Carlo, S. Bellani, F. Bonaccorso, Low-temperature graphene-based paste for large-area carbon perovskite solar cells, ACS Appl. Mater. Interfaces 13 (2021) 22368–22380.
[15] A.G.M. Ferrari, H.M. Elbardisy, V. Silva, T.S. Belal, W. Talaat, H.G. Daabees, C. E. Banks, D.A. Brownson, The influence of lateral flake size in graphene/graphite paste electrodes: an electroanalytical investigation, Anal. Methods 12 (2020) 2133–2142.
[16] D.S. Rana, R. Sharma, S. Kumar, N. Gupta, S. Thakur, K.K. Thakur, D. Singh, Molybdenum disulfide (MoS2) and reduced graphene oxide (rGO) nanocomposite based electrochemical sensor for detecting mercury (II) ions, Nano-Structures & Nano-Objects 36 (2023) 101041.
[17] E. Mahmud, M.R. Islam, Improved electrochemical performance of bio-derived plasticized starch/reduced graphene oxide/molybdenum disulfide ternary nanocomposite for flexible energy storage applications, Sci. Rep. 13 (2023) 20967.
[18] K. Ahmad, M.A. Shinde, H. Kim, Molybdenum disulfide/reduced graphene oxide: progress in synthesis and electro-catalytic properties for electrochemical sensing and dye sensitized solar cells, Microchem. J. 169 (2021) 106583.
[19] N.E. Safie, M.A. Azam, Understanding the structural properties of feasible chemically reduced graphene, AIMS Materials Science 9 (2022) 617–627.
[20] N.E. Safie, M.N.F.M. Sairi, M.A. Azam, A. Takasaki, Development and analysis of rGO-MoS2 nanocomposite as top electrode for the application of inverted planar perovskite solar cells via SCAPS-1D device simulation, J. Mater. Res. 37 (2022) 3372–3383.
[21] J.H. Gosling, O. Makarovsky, F. Wang, N.D. Cottam, M.T. Greenaway, A. Patanè, R. D. Wildman, C.J. Tuck, L. Turyanska, T.M. Fromhold, Universal mobility characteristics of graphene originating from charge scattering by ionised impurities, Commun. Phys. 4 (2021) 30.
[22] R. Wang, R. Moos, Electrical conductivity determination of semiconductors by utilizing photography, finite element simulation and resistance measurement, J. Mater. Sci. 56 (2021) 10449–10457.
[23] Z. Wang, H. Dong, Y. Zou, Q. Zhao, J. Tan, J. Liu, X. Lu, J. Xiao, Q. Zhang, W. Hu, Soft-etching copper and silver electrodes for significant device performance improvement toward facile, cost-effective, bottom-contacted, organic field-effect transistors, ACS Appl. Mater. Interfaces 8 (2016) 7919–7927.
[24] B. Fu, C. Deng, L. Yang, Efficiency enhancement of solid-state CuInS2 quantum dot-sensitized solar cells by improving the charge recombination, Nanoscale Res. Lett. 14 (2019) 198.
[25] J.H. Choi, M.C. Kim, S.H. Moon, H. Kim, Y.S. Kim, K.W. Park, Enhanced electrochemical performance of MoS2/graphene nanosheet nanocomposites, RSC Adv. 10 (2020) 19077–19082.
[26] P. Kajal, J.H. Lew, A. Kanwat, P.J.S. Rana, G.V. Nutan, T.M. Koh, S.G. Mhaisalkar, S. Powar, N. Mathews, Unveiling the role of carbon black in printable mesoscopic perovskite solar cells, J. Power Sources 501 (2021) 230019.
[27] A.K. Gautam, M. Faraz, N. Khare, Enhanced thermoelectric properties of MoS2 with the incorporation of reduced graphene oxide (RGO), J. Alloys Compd. 838 (2020) 155673.
[28] J. Chen, Y. Xia, J. Yang, B. Chen, Fabrication of monolayer MoS 2/rGO hybrids with excellent tribological performances through a surfactant-assisted hydrothermal route, Appl. Phys. A 124 (2018) 1–8.
[29] H. Guo, L. Wang, W. You, L. Yang, X. Li, G. Chen, Z. Wu, X. Qian, M. Wang, R. Che, Engineering phase transformation of MoS2/RGO by N-doping as an excellent microwave absorber, ACS Appl. Mater. Interfaces 12 (2020) 16831–16840.
[30] K.D. Rasamani, F. Alimohammadi, Y. Sun, Interlayer-expanded MoS2, Mater. Today 20 (2017) 83–91.
[31] A. Deshpande, K. Hojo, K. Tanaka, P. Arias, H. Zaid, M. Liao, M. Goorsky, S. Kodambaka, Need for complementary techniques for reliable characterization of MoS2-like layers, J. Vac. Sci. Technol. A 41 (2023).
[32] H. Wördenweber, A. Grundmann, Z. Wang, S. Hoffmann-Eifert, H. Kalisch, A. Vescan, M. Heuken, R. Waser, S. Karthäuser, The MoS2-graphene-sapphire heterostructure: influence of substrate properties on the MoS2 band structure, J. Phys. Chem. C 127 (2023) 10878–10887.
[33] M.S. Shamna, K.S. Nithya, K.S. Sudheer, Simulation and optimization of CH3NH3SnI3 based inverted perovskite solar cell with NiO as Hole transport material, Mater. Today: Proc. 33 (2020) 1246–1251.
[34] E. Widianto, E.S. Rosa, K. Triyana, N.M. Nursam, I. Santoso, Performance analysis of carbon-based perovskite solar cells by graphene oxide as hole transport layer: experimental and numerical simulation, Opt. Mater. 121 (2021) 111584.
[35] B. Sharma, A.S. Mathur, V.K. Rajput, I.K. Singhand, B.P. Singh, Device modeling of non-fullerene organic solar cell by incorporating CuSCN as a hole transport layer using SCAPS, Optik 251 (2022) 168457.
[36] V.D. Dang, C.Y. Hsiao, P.A. Le, V.Q. Le, D. Ho Phuong Thao, T.H. Do, K.H. Wei, Surface-plasma-induced one-pot synthesis of N, S-carbon dot intercalated MoS2/graphene nanosheets for highly efficient hydrogen evolution reaction, ACS Appl. Energy Mater. 5 (2022) 12817–12827.
[37] N. Joseph, P.M. Shafi, A.C. Bose, Recent advances in 2D-MoS2 and its composite nanostructures for supercapacitor electrode application, Energy Fuels 34 (2020) 6558–6597.
[38] C. Guo, C. Wang, H. Sun, D. Dai, H. Gao, A simple electrochemical sensor based on rGO/MoS 2/CS modified GCE for highly sensitive detection of Pb (ii) in tobacco leaves, RSC Adv. 11 (2021) 29590–29597.
[39] K. Ramakrishnan, C. Nithya, R. Karvembu, Heterostructure of two different 2D materials based on MoS 2 nanoflowers@ rGO: an electrode material for sodium-ion capacitors, Nanoscale Adv. 1 (2019) 334–341.
[40] X. Bai, T. Cao, T. Xia, C. Wu, M. Feng, X. Li, Z. Mei, H. Gao, D. Huo, X. Ren, S. Li, MoS2/NiSe2/rGO multiple-interfaced sandwich-like nanostructures as efficient electrocatalysts for overall water splitting, Nanomaterials 13 (2023) 752.
[41] P. Kajal, J.H. Lew, A. Kanwat, P.J.S. Rana, G.V. Nutan, T.M. Koh, S.G. Mhaisalkar, S. Powar, N. Mathews, Unveiling the role of carbon black in printable mesoscopic perovskite solar cells, J. Power Sources 501 (2021) 230019.
[42] S. He, L. Qiu, D.Y. Son, Z. Liu, E.J. Juarez-Perez, L.K. Ono, C. Stecker, Y. Qi, Carbon-based electrode engineering boosts the efficiency of all low-temperature-processed perovskite solar cells, ACS Energy Lett. 4 (2019) 2032–2039.
[43] V. Babu, R. Fuentes Pineda, T. Ahmad, A.O. Alvarez, L.A. Castriotta, A. Di Carlo, F. Fabregat-Santiago, K. Wojciechowski, Improved stability of inverted and flexible perovskite solar cells with carbon electrode, ACS Appl. Energy Mater. 3 (2020) 5126–5134.